Author/s:
Bye, JAT;Wolff, JO;Lettmann, KA

Title:
A note on ocean surface drift with application to surface velocities measured with HF Radar

Date:
2017-08-01

Citation:
Bye, J. A. T., Wolff, J. O. & Lettmann, K. A. (2017). A note on ocean surface drift with application to surface velocities measured with HF Radar. Journal of Oceanography, 73 (4), pp.491-502. https://doi.org/10.1007/s10872-017-0417-1.

Persistent Link:
https://hdl.handle.net/11343/283298

A Note on ocean surface drift with application to surface velocities measured with HF Radar

John A.T. Bye[1], Jörg-Olaf Wolff[2] and Karsten A. Lettmann[2]

[1] School of Earth Sciences, The University of Melbourne, Victoria 3010, Australia

jbye@unimelb.edu.au, T: 618 8558 3705, F: 613 8344 7761

[2] ICBM, Carl-von-Ossietzky Universität Oldenburg, Postfach 2053, 26111 Oldenburg, Germany

Abstract The ocean drift current consists of a (local) pure drift current generated by the interaction of the wind and waves at the sea surface, to which is added vectorially the surface geostrophic current. We present, (a) a similarity solution for the wave boundary layer (which has been validated through the prediction of the 10m drag law) from which the component of pure drift current along the direction of the wind (and hence the speed factor) can be evaluated from the 10m wind speed and the peak wave period, and (b) a similarity solution for the Ekman layers of the two fluids which shows that under steady-state neutral conditions the pure drift current lies along the direction of the geostrophic wind, and has a magnitude 0.034 that of the geostrophic wind speed. The co-existence of these two similarity solutions indicates that the frictional properties of the coupled air-sea system are easily evaluated functions of the 10m wind speed and the peak wave period, and also leads to a simple expression for the angle of deflection of the pure drift current to the 10m wind. The analysis provides a dynamical model for global ocean drift on monthly and annual time scales for which the steady-state neutral model is a good approximation. In particular, the theoretical results appear to be able to successfully predict the mean surface drift measured by HF Radar, which at present is the best technique for studying the near surface velocity profile.

Keywords global surface ocean drift, wave boundary layer, Ekman layers, aerodynamically rough flow, surface geostrophic current, similarity analysis, HF Radar measurements

1. Introduction

Ocean surface drift is a fundamental element of the geophysical fluid dynamics of both the ocean and the atmosphere. Hence its understanding requires a model of the near surface flow in both fluids. Here we introduce a similarity model of the sea surface drift which takes account of the wave dynamics and also of the turbulence in the Ekman layers of the two fluids, through which a relation for the angle of turning of the surface drift to the surface shear stress is obtained. The model uses the wind speed and the peak wave period to predict the 'pure surface drift' which is the surface drift current relative to the surface geostrophic current ($\underline{u}_0$), which is the reference velocity for the dynamics of the air-sea boundary layer.

The predictions apply strictly to homogeneous steady-state conditions in both air and water, which are approximately satisfied in observational studies that have been undertaken to derive the 10m drag law and typically use a time scale of averaging between 10 and 30 minutes. In the extension to the Ekman layer however longer time scales of averaging are implicitly assumed in the prediction for the angle of turning.

Section 2 summarizes the basic properties of the similarity model, which takes account of the three main processes that control the air-sea boundary layer, namely, wave generation, frictional drag, and the production of spray, with associated white capping and slip. There are no disposable constants in the model which is centered on the interaction of the above three processes within the similarity regime of air and water as they interact at the sea surface.

The similarity model (Bye 1995; Bye 2002), which was extended in Bye and Jenkins (2006), Bye and Wolff (2008) and Bye et al. (2010) to include conditions at very high wind speeds, has recently been shown to predict an expression for the 10m drag coefficient (Bye et al. 2014) in

excellent agreement with the consolidated sets of observational data summarized in Foreman and Emeis (2010) and Andreas et al. (2012) over the mid-range of wind speeds (5 – 17 ms^{-1}). At low wind speeds however there is a scatter in the observational estimates of the 10m drag coefficient as shown, for example, in Yelland and Taylor (1996), the significance of which is discussed in Section 5.2.

Here, we show how the similarity model can be used to obtain various expressions relevant to the ocean drift circulation. An important feature of the model is the representation of the near surface velocity in the water by two components; one due to the wave field and one due to turbulence. In steady conditions in the open ocean, as discussed in Section 3.5, the turbulent component normally transfers momentum downwards into the Ekman layer where it is dissipated.

The dynamics of the wave boundary layer in the water are very different from those in the air, principally because the phase velocities of the waves are important in the atmosphere whereas the particle velocities are important in the ocean. The overriding hypothesis however is that when both components of velocity are included in the oceanic boundary layer, the oceanic shear can be related by a similarity argument to the atmospheric shear. The spanwise structure of the turbulence which gives rise to the Langmuir circulation is not of primary importance in this similarity model.

In the application of the similarity model we assume a unimodal wave spectrum in which a unique peak wave number can be identified. Thus there are two variables in the model; the wind speed and the peak wave period. The 10m wind speed is assumed to be greater than about 3 m s^{-1} at which the onset of wave growth occurs, and the range of applicability of peak wave period is discussed in Section 3.1.

In Sections 3.1 and 3.2 the results of the similarity model are applied to obtain expressions for the surface drift current, and in Section 3.3 the key result from the similarity theory for the coupled Ekman layers, that the pure drift lies along the direction of the surface geostrophic wind is presented. In Section 3.4 an expression for the angle of deflection of the pure surface drift to the surface shear stress is derived. Section 4 considers near surface drift, which is important for the transport of surface trapped buoyant material (Section 4.1) and also for the interpretation of the drift derived from HF Radar studies (Section 4.2).

Section 5 takes a look at two important sets of drift observations, a classical drift card study in the North Atlantic Ocean (Section 5.1) and recent HF Radar surface drift measurements in the coastal seas of Japan (Section 5.2), which are interpreted in terms of the theoretical model.

Section 6 is a summary of the main features of the analysis, which emphasizes the perspective from which this work has evolved in comparison with other studies.

In essence our model provides a seamless transition from the frictionless environment of the atmosphere specified by the local surface geostrophic velocity, to that of the ocean specified by the surface geostrophic current, which is the reference current for the planetary boundary layer dynamics. The effects of stratification are not explicitly taken into account as the focus of the analysis is the importance of the wave field.

The symbols used in the analysis, which are fully defined in the text, are also summarized in the Glossary at the end of the paper.

2. The similarity theory

The similarity equations for the surface shear stress ($\underline{\tau}_s$) are the following (Bye and Wolff 2008). In the air,

$$\underline{\tau}_s = \rho_1 |\underline{u}_*|\underline{u}_* = \rho_1 K | \underline{u}(z) - \underline{u}_o - \underline{u}_L | (\underline{u}(z) - \underline{u}_o - \underline{u}_L) \qquad (1)$$

and in the water,

$$\underline{\tau}_s = \rho_2 |\underline{w}_*|\underline{w}_* = \rho_2 K |\varepsilon\underline{u}_L - \underline{u}(-z) + \underline{u}_o | (\varepsilon\underline{u}_L - \underline{u}(-z) + \underline{u}_o) \qquad (2)$$

where oz is vertically upwards, and z = 0 denotes the mean interfacial level. The densities of air and water are respectively, ρ_1 and ρ_2 , $\varepsilon = (\rho_1/\rho_2)^{1/2}$, and $\underline{u}_*$ and $\underline{w}_*$ are the corresponding friction velocities. The air velocity at height z is u(z), and the water velocity at depth –z is $\underline{u}(-z)$. $\underline{u}_o$ is the oceanic reference velocity at the base of the air-sea boundary layer. $\underline{u}_L$ is the wave-induced velocity in the air, which is due to the spectrally weighted phase velocities, and $\varepsilon\underline{u}_L$ is the wave-induced velocity in the water, which is due to the spectrally integrated particle velocities. $\underline{u}_L$ and $\varepsilon\underline{u}_L$ occur at the inner edge of the wave boundary layer, $|\underline{z}| = z_R$. Therefore, in the similarity hypothesis, the drag laws (Eqs. (1) and (2)) are constructed relative to the wave-induced velocities in air and water, which are assumed to be in the ratio 1: ε. $K = K(|\underline{z}|)$ is a drag coefficient which is equal in the two fluids at the same vertical distance from the undisturbed sea surface, and assumed to be applicable under aerodynamically rough conditions in which the viscosities of the two fluids are not relevant quantities.

For $\underline{u}o = 0$, $\underline{\tau}_s$ is determined solely by the local conditions ($\underline{u}(z)$, $\underline{u}(-z)$ and $\underline{u}_L$) and gives rise to the pure drift circulation. The complete drift circulation is obtained by simply adding $\underline{u}_o$ to the pure drift circulation in which, for steady horizontally homogeneous conditions $\underline{u}_o$ is the surface geostrophic current. In the following analysis, unless specifically noted, we consider the pure drift circulation for which the similarity expressions in (1) and (2) are,

$$\underline{\tau}_s = \rho_1 K | \underline{u}(z) - \underline{u}_L | (\underline{u}(z) - \underline{u}_L) \qquad (3)$$

and,

$$\underline{\tau_s} = \rho_2 K \,|\, \varepsilon \underline{u}_L - \underline{u}(-z) \,|\, (\varepsilon \underline{u}_L - \underline{u}(-z)) \qquad (4)$$

On combining (3) at z, with (4) at -z, we obtain the ancillary relations, $\underline{\tau}_s = \rho_1 (¼ K) \,|\, \underline{u}(z) - \underline{u}(-z)/\varepsilon| \,(\underline{u}(z) - \underline{u}(-z)/\varepsilon)$ and $\varepsilon\underline{u}_L = ½ (\varepsilon\underline{u}(z) + \underline{u}(-z))$ which are assumed to extend to the edge of the boundary layer significantly influenced by the wave motion which occurs at $|z| = z_B$, where $z_B = 1/(2k_0)$ in which k_0 is the wave number of the peak wave. Thus for $|z| > z_B$, the velocities in each fluid are assumed to be controlled by turbulent rather than wave processes.

On evaluating the ancillary relations at z_B , we obtain,

$$\underline{u}_* = K_I^{1/2} \,(\underline{u}_1 - \underline{u}_2/\varepsilon) \qquad (5)$$

and

$$\varepsilon \underline{u}_L = ½ \,(\varepsilon\underline{u}_1 + \underline{u}_2) \qquad (6)$$

where $\underline{u}_1 = \underline{u}(z_B)$ and $\underline{u}_2 = \underline{u}(-z_B)$ respectively are defined as the surface wind and the surface current, and $K_I = ¼ K(|z_B|)$. Figure 1, which is reproduced from Fig. 1 in Bye and Wolff (2008) illustrates the velocity structure. The evaluation and significance of K_I is discussed in Section 3.3.

Eq. (5) has the property that the interaction between the surface wind and the surface current is governed by the inertially weighted shear $(\underline{u}_1 - \underline{u}_2/\varepsilon)$ rather than by a simple linear shear. However, if the two fluids are of equal density, the Newtonian linear shear is recovered.

3. The surface drift current

At the sea surface on defining the surface drift velocity ($\underline{u}_s$) by equating the air velocity and the water velocity in the second ancillary at z = 0, we have that,

$$\underline{u}_s = 2\varepsilon/(1+\varepsilon)\,\underline{u}_L \qquad (7)$$

which shows since $\varepsilon << 1$, that $\underline{u}_s$ is approximately twice the wave-induced velocity ($\varepsilon\underline{u}_L$). From (6) we also have, $2\varepsilon\,\underline{u}_L = \varepsilon\,\underline{u}_1 + \underline{u}_2$ and hence in terms of the surface wind and current,

$$\underline{u}_s = 1/(1+\varepsilon)\,(\varepsilon\,\underline{u}_1 + \underline{u}_2) \qquad (8)$$

Using (5), expressions for $\underline{u}_s$ in terms of atmospheric quantities only and oceanic quantities only can also be derived from (8) which are respectively,

$$\underline{u}_s = \varepsilon/(1+\varepsilon)\,(2\,\underline{u}_1 - \underline{u}_*/K_I^{1/2}) \qquad (9)$$

and

$$u_s = 1/(1+\varepsilon)\,(2\,\underline{u}_2 + \underline{w}_*/K_I^{1/2}) \qquad (10)$$

3.1 The component of the pure surface drift parallel to the surface shear stress

We use (9) to obtain an expression for the pure surface drift in terms of atmospheric data by resolving along the direction of the surface stress, and assuming that in the air neutral conditions apply. Then on the assumption that $\underline{\tau}_s$ lies along ox, and that the wind profile is locally logarithmic, we have, $u_1 = u_{10} + u_*/\kappa \ln(z_B/z_{10})$ where $\kappa = 0.4$ is von Karman's constant, $z_{10} =$ 10 m, and u_{10} is the 10 m wind speed. On now expressing the peak wavenumber (k_o) in terms of the peak wave period (T), we obtain $z_B = g\,T^2/8\pi^2$ in which $g = 9.8\ ms^{-2}$ is the acceleration of gravity. Hence, on substituting for u_1 in the ox-component of (9), $u_s = \varepsilon/(1+\varepsilon)\ [\,2\,u_{10} + 2\,u_*/\kappa \ln(gT^2/8\pi^2 z_{10}) - u_*/K_I^{1/2}\,]$, which, on using the drag relation $u_*^2 = K_{10}\,u_{10}^2$ where K_{10} is the 10m drag coefficient, yields the speed factor,

$$u_s/w_* = 1/(1+\varepsilon)\ (2R-1)/K_I^{1/2} \qquad (11)$$

where

$$R = K_I^{1/2}/\kappa \; [\kappa/K_{10}^{1/2} + \ln (gT^2/8\pi^2 z_{10})] \qquad (12)$$

is a frictional parameter which can be evaluated for a peak wave period (T) and a friction velocity (u_*) using the 10m drag relation ($K_{10}(u_{10})$) . The logarithmic interpolation over the height range from z_B to z_{10} used in the derivation of (12) is likely to be a good approximation (neglecting any effects of atmospheric stability) if the reference height lies well beyond the dynamical effects of the wave field. This restriction can be investigated using the wave breaking criterion, $a_o k_o = ¼$, where a_o is the amplitude of the breaking wave (Pond and Pickard 1983). For $a_o < z_{10}$, we require that for a breaking peak wave, $T < 4\pi (z_{10}/g)^{1/2} \approx 13$ s , which is satisfied in most sea states.

This suggests that (12) is a robust expression that may be applied quite generally. The two terms in the bracket indicate that R increases as K_{10} decreases and also as T increases. In particular, the combination of low wind speeds and high peak wave periods, such as occurs in a swell dominated environment gives rise to relatively large values of R. Here we evaluate R (Figure 2(a)) from the similarity model using equation (A1) in the Appendix of Bye et al. (2014) in which the drag coefficient maximum ($K_{10m} = 0.002$) at which the 10m wind speed, $u_{10m} = 40$ ms^{-1}. The application of the similarity model in evaluating K_{10}, which was shown to be in excellent agreement with observations over the range, $5 < u_{10} < 17$ ms^{-1}, is fully described in Bye at al. (2014).

The importance of R in determining the speed factor (u_s/w_*) through (11), is illustrated in Figure 2(b), which shows that u_s/w_* increases as u_* decreases and T increases. R is also significant for the evaluation of the angle of deflection (32) of the pure drift current from the surface shear

stress, which from (7) is also the angle of deflection of the wave-induced velocity in the water, as discussed in Section 3.5.

3.2 The component of the pure surface drift normal to the surface shear stress

Normal to the surface shear stress $v_* = 0$, and from (3) and (4) respectively $v(z) = v_L$ and $v(-z) = \varepsilon v_L$. These relations show that the normal components of velocity in the wave boundary layer are independent of depth. Hence the normal components of the surface wind velocity ($v_1 = v(z)$) and the surface current velocity ($v_2 = v(-z)$) are identical with the corresponding components of wave-induced velocities, v_L and εv_L, and since u(z) increases with height whilst v(z) remains constant, it is also clear that the angle of deflection of the air velocity decreases with height so that in the pure drift circulation $\underline{u}(z)$ is always directed at an angle intermediate between the surface shear stress and the wave field.

In the field studies of Geernaert (1988) and Rieder et al.(1994), which are discussed in Friehe et al. (2001), however, a swell from a distant source occurred at the measurement site and the direction of the wind stress was observed to be intermediate between the wind direction and the direction of propagation of the swell. We suggest that in this situation the surface shear stress may have been rotated to oppose the incoming swell without a change in wind direction, as demonstrated by (3) for a swell approaching normal to the wind direction..

3.3 The evaluation and significance of the inertial drag coefficient

The inertial drag coefficient was first evaluated in Bye and Wolff (2004) by comparison of the theoretical expression for K_{10},

$$K_{10}^{-1/2} = K_I^{-1/2} - 1/\kappa \ln c u_*^2 \qquad (13)$$

where $c = 1/(2A^2 g z_{10}) = 6\ m^{-2}s^{-1}$, with the experimental data for the growing wind-wave sea over the wind speed range, $5 \leq u_{10} \leq 30\ ms^{-1}$ presented in Garratt (1977). This comparison yielded $K_I = 0.0015$. Eq. (13) was derived by assuming that the growing wind-wave sea has the property that the velocity shear in the water is totally caused by the wave motion, i.e. $u_2 = 0$ in (5), and that the expression of Toba (1973) for the fully developed growing wind wave sea, $2\pi/T = Ag/u_*$ in which $A = 0.029$ is applicable.

In Bye and Wolff (2004) it was also shown for the Toba (1973) wavenumber spectrum, that,

$$K_I = [2 \ln(k_1/k_o)/\kappa]^{-2} \qquad (14)$$

where $k_1 = 1/(2z_R)$ is the spectral high wavenumber cut-off, and $k_o = 1/(2z_B)$ is the wave number of the peak wave. Eq. (14) follows from the logarithmic evaluation of (3) at $z = z_B$. Hence K_I is a property of the extent of the wave spectrum. For $K_I = 0.0015$, $k_1/k_o \approx 180$ such that the Stokes drift due to the wave spectrum occurs over approximately two decades in wavenumber space.

3.4 The similarity model for the coupled Ekman layers

We now consider the consequences of the co-existence of the similarity solution in the wave boundary layer of both fluids, with another similarity solution for the Ekman layers of both fluids

in each of which the eddy viscosity is assumed to be constant as in the original analysis of Ekman (1905). This solution, which was presented in Bye (2002), is,

$$\underline{\tau}_s = Q_1 [(-u_1' + v_1') , (- u_1' - v_1')]$$

$$= Q_2 [(u_2' - v_2') , (u_2' + v_2')] \qquad (15)$$

where $\underline{u}_1' = - \underline{u}_g + \underline{u}_1$ and $\underline{u}_2' = - \underline{u}_o + \underline{u}_2$ are the frictional velocities in air and water respectively, $\underline{u}_g$ is the surface geostrophic wind and $\underline{u}_o$ is the oceanic surface geostrophic velocity, and for pure surface drift, $\underline{u}_0 = 0$. In the northern hemisphere ($f > 0$), the friction coefficients are, $Q_1 = \rho_1 (f\nu_1/2)^{1/2}$ and $Q_2 = \rho_2 (f\nu_2/2)^{1/2}$ in which $f = 2\Omega \sin\varphi$ is the Coriolis parameter, where Ω is the angular speed of rotation of the Earth and φ is latitude, and ν_1 and ν_2 are the respective constant fluid viscosities.

On assuming that $\underline{\tau}_s$ lies along ox as before, $u_1' + v_1' = 0$ and $u_2' + v_2' = 0$, and hence,

$$\underline{u}_1' = - \tfrac{1}{2} (1, -1) \tau_{sx}/Q_1 \qquad (16)$$

$$\underline{u}_2' = \tfrac{1}{2} (1, -1) \tau_{sx}/Q_2 \qquad (17)$$

On now applying the similarity expressions for fully turbulent flow in which $\nu_1 = G\kappa u_*^2/f$ and $\nu_2 = G\kappa w_*^2/f$ and G is a non-dimensional constant of $O(10^{-1})$ (Garratt 1992) we obtain,

$$Q_1 = \varepsilon Q_2 \qquad (18)$$

where $Q_1 = \rho_1 (G\kappa/2)^{1/2} u_*$. On substituting (18), (15) yields the similarity relation,

$$\varepsilon \underline{u}_1' + \underline{u}_2' = 0 \qquad (19)$$

from which on substituting for $\underline{u}_1$ and $\underline{u}_2$ in (8) using (19) we obtain,

$$\underline{u}_s = \varepsilon/(1 + \varepsilon) (\underline{u}_g - \underline{u}_0) + \underline{u}_0 \qquad (20)$$

In (20), the first term is an expression for the pure surface drift current in terms of the surface geostrophic wind relative to the surface geostrophic current, and the second term is the surface geostrophic current. For $\underline{u}_o = 0$, (20) reduces to the relation,

$$\underline{u}_s = \varepsilon/(1 + \varepsilon)\, \underline{u}_g \qquad (21)$$

such that the pure drift current lies along the direction of the surface *geostrophic* wind, and since $\varepsilon << 1$ ($\rho_1 = 1.2$ kgm^{-3}, $\rho_2 = 1025$ kgm^{-3}), the speed of the pure drift current is 0.034 that of the geostrophic wind speed. This simple result, which depends only on the similarity relation (19), indicates that in the northern hemisphere, the deflection of the surface shear stress to the left hand side of the geostrophic wind is exactly compensated in the pure surface drift by an identical deflection to the right hand side of the surface shear stress, see Section 3.5. In the southern hemisphere the signs of these two deflections are reversed.

On substituting for $\underline{u}_s$ from (7) in (21), a corollary result is,

$$\varepsilon\, \underline{u}_L = \tfrac{1}{2}\, \varepsilon\, \underline{u}_g \qquad (22)$$

which shows that in a neutral Ekman layer, the wave-induced velocity ($\varepsilon\, \underline{u}_L$) would also be proportional to the surface geostrophic wind ($\underline{u}_g$).

3.5 The magnitude of the deflection

On returning to (16) and (17) and substituting for Q_1 and Q_2 from (18) we obtain,

$$(u_1', v_1') = \tfrac{1}{2}\, u_* (-1, 1) / (\alpha K_I^{1/2}) \qquad (23)$$

and

$$(u_2', v_2') = \tfrac{1}{2}\, w_* (1, -1) / (\alpha K_I^{1/2}) \qquad (24)$$

where

$$\alpha = (G\kappa/2K_I)^{1/2} \qquad (25)$$

from which on assuming that $\underline{u}_0 = 0$, such that the expressions apply directly to pure drift, and substituting (23) and (24) in (5), we obtain,

$$u_g = (1 + \alpha)/\alpha\ \ u_*/K_I^{1/2} \qquad (26)$$

and

$$v_g = - 1/\alpha \; u_*/K_I^{1/2} \qquad (27)$$

In these expressions α is a non-dimensional parameter arising from the fully turbulent conditions in the coupled Ekman layers.

The component of pure drift along ox, from (21), is $u_s = \varepsilon/ (1 + \varepsilon) u_g$. Hence on substituting for u_g from (26) we have,

$$u_s = 1/(1 + \varepsilon) (1 + \alpha)/\alpha \;\; w_*/K_I^{1/2} \qquad (28)$$

Similarly, from (21) the normal component of pure drift, $v_s = \varepsilon/ (1 + \varepsilon) v_g$, which from (27), yields,

$$v_s = - 1/(1 + \varepsilon) \;\; 1/\alpha \;\; w_*/K_I^{1/2} \qquad (29)$$

For the co-existence of both similarity solutions, the expression (28) for u_s must be identical with (11), thus $(1 + \alpha)/\alpha = 2R - 1$, and hence,

$$\alpha = ½ /(R - 1) \qquad (30)$$

which shows that: (i) in the coupled Ekman layers α is determined by R which is a function of the wind and wave conditions, and (ii) steady coupled Ekman layers can only exist if $R > 1$ ($\alpha > 0$). Eq. (30) can be obtained directly by equating of the frictional velocities along ox at z_B in the Ekman layer and in the wave boundary layer, which are respectively, $½ \; w_*/ (\alpha \; K_I^{1/2})$ from (24) and $w_* (R - 1)/ K_I^{1/2}$ from (10) using (11). The physical processes in the wave boundary layer which occur when $R > 1$ are discussed in Section 3.6.

On substituting for α using (30) in (26) and (27) we obtain the geostrophic drag coefficient, $K_0 = u_*^2/(v_g^2 + u_g^2) = K_I / [(2R - 1)^2 + 4 (R - 1)^2]$, $R > 1$, and the angle of turning of the surface geostrophic wind to the left hand side of the surface shear stress,

$$\gamma = \tan^{-1} (v_g/u_g) = - \tan^{-1} [(R- 1) /(R - ½)] \quad , \qquad R > 1 \qquad (31)$$

and from (28) and (29) the angle of deflection of the pure surface drift to the left hand side of the surface shear stress,

$$\gamma = \tan^{-1}(v_s/u_s) = -\tan^{-1}[(R-1)/(R-\tfrac{1}{2})] \quad , \qquad R > 1 \qquad (32)$$

has an identical value, and hence the pure surface drift lies along the direction of the surface geostrophic wind as in (21). . For $R > 1$, in the northern hemisphere, $\gamma < 0$, as in (31) and (32), whereas $\gamma > 0$ in the southern hemisphere, as illustrated in Figure 3.

The variation of γ with u_* and T is only shown for $R \geq 1$ in Figure 3, since for $R < 1$, (30) shows that a steady-state Ekman layer does not exist. In the limit of $R \rightarrow 1$, $\alpha \rightarrow \infty$, and the frictional velocities in the Ekman layers ($\underline{u}_1' \rightarrow 0$ and $\underline{u}_2' \rightarrow 0$), and ($u_g \rightarrow u_*/K_I^{1/2}$, $v_g \rightarrow 0$), i.e the Ekman layer vanishes.

Sea states in which $R < 1$, many of which are illustrated in Figure 1 of Bye et al. (2010), reflect unsteady conditions during the impulsive generation of the growing wind-wave sea. In these conditions ($R \leq 1$), we anticipate that the normal component of velocity in the wave boundary layer is zero, and hence $\gamma = 0$, and also $K_0 = K_I / (2R-1)^2$

3.6 Momentum transfers by slip and wave breaking

On substituting for u_2 in (10) from (11), and for εu_L in (7) from (11), we have $u_2 = w_*(R\text{-}1) / K_I^{1/2}$ which is the velocity in the wave boundary layer due to turbulence, and $\varepsilon u_L = \tfrac{1}{2} w_*(2R-1) / K_I^{1/2}$ which is the wave-induced velocity. The difference between these two velocities, $u_{St} = \varepsilon u_L - u_2$, is the surface Stokes velocity.

For R > 1, the turbulent velocity is positive ($u_2 > 0$) due to slip. For R < 1, the turbulent velocity is negative ($u_2 < 0$) due to wave breaking. For R = 1, the effects of wave breaking and slip are in balance.

In the wave boundary layer, the oceanic shear is $u_{St} = ½ w_* / K_I^{1/2}$ (since the Stokes velocity is zero at the lower boundary, and the turbulent velocity is constant throughout), and from (3) the atmospheric shear is $u_1 - u_L = ½ u_* / K_I^{1/2}$. Hence the shears in the two fluids along ox are in the ratio, $\varepsilon : 1$ in agreement with the similarity hypothesis of (3) and (4) .

4. Near surface drift

In the previous discussion in Section 3.4, the only aspect of the circulation normal to the surface stress that has been considered is that due to the Earth's rotation. The Langmuir circulation, see for example, Thorpe (2004), is also present, and indeed was decisive in aligning the drift floats of various lengths which were used in the experiments (Bye 1965 and 1987) from which the similarity model (Bye 1988 and 2005) was developed. Hence our analysis applies specifically to a sample of the water surface in which a convergent lateral circulation occurs which carries the drift of near surface material. We emphasize that the similarity model used in the theoretical formulation of the pure drift circulation in the wave boundary layer, which is fundamentally Lagrangian, implicitly incorporates the effects of the Langmuir circulation.

Pure surface drift, the properties occurs at the sea surface. In practice, near surface drift is often the more relevant process. Two important instances are discussed respectively in: 4.1 the surface drift layer, in which wave breaking occurs, and 4.2 HF Radar mean drift, in which HF

Radar measurements sample a deeper layer. The mean drift in these two layers can be evaluated by assuming the existence of a logarithmic near surface velocity profile,

$$u(z) = u_s - w_*/\kappa \ln z/z_s \qquad (33)$$

where z is vertically downwards and z_s is the roughness length relative to the pure surface drift current (u_s). On integrating (33) over the depth range (z_s, z) we obtain a mean drift current,

$$\langle u \rangle \approx u_s + w_*/\kappa \, (1 - \ln z/z_s) \qquad (34)$$

4.1 The surface drift layer

It is commonly observed that neutrally buoyant objects drifting near the sea surface are subject to tumbling motions due to breaking waves and turbulence which intermittently draw them down into the water column where the forward motion is smaller than at the sea surface. This process can be incorporated into the drift model by averaging the near surface velocity profile over the depth of the surface drift layer in which the neutrally buoyant material may be expected to be transported. This surface drift layer is assumed to occur over the depth range in which the mean velocity is reduced from the surface drift velocity ($2\varepsilon/(1 + \varepsilon)\ \underline{u}_L$) to the wave-induced velocity ($\varepsilon \underline{u}_L$). This model is based on the small scale drift measurements in Bye (1987), which were analyzed in Bye (1988), and also on an extensive series of long term drift observations with drift cards in the Southern Ocean (Bye 2012) which initiated this theoretical study.

On substituting $u(z) \approx \frac{1}{2}\, u_s$ in (33) and substituting for u_s from (11), (34) yields the speed factor for the mean drift current in the surface drift layer,

$$u_d / w_* \approx [(\tfrac{1}{2}\,(2R-1) + K_I^{1/2}/\kappa]/K_I^{1/2} \qquad (35)$$

where $u_d = \langle u \rangle$, and from (7) $\underline{u}_d$ and $\underline{u}_s$ lie in the same direction. In an idealized case study in which $G \approx 0.1$ (Garratt, 1992) the properties of the surface drift layer are the following:

(i) from (25), $\alpha \approx 3.7$, and hence from (30) the frictional parameter $R \approx 1.1$.

(ii) from (11) and (35), the ratio, $u_d/u_s \approx 0.6$, which is similar to the ratio observed in the field experiments (Bye 1965, 1987), i.e. the effective drift velocity for tumbling material in the surface drift layer is about 60% that of the pure surface drift velocity..

(iii) from (31) or (32), $\gamma \pm 9^o$. , and hence u_s rotated through the angle γ , is normally a sufficiently accurate relation for the speed of the pure drift circulation.

(iv) from (35), $u_d \approx 18\, w_*$, and from (24), $v_2 \approx -\, 4\, w_*$

4.2 HF Radar mean drift

In the second application we consider the mean drift over a deeper layer which extends downwards to z_{HF} over which the HF Radar measurements are assumed to extend, and define the ratio, $\varphi = z_{HF}/z_B$, where z_B is the depth of the wave boundary layer. On substituting $z = z_{HF}$ in (34) the HF radar mean drift current, $u_{HF} \approx u_s + w_*/\kappa\, (1 - \ln \varphi - \ln z_B/z_s)$ in which from (33) , $u_s - w_*/\kappa \ln z_B/z_s = u_2$. Hence on substituting for u_2 the speed factor for the HF Radar derived mean drift current is,

$$u_{HF} / w_* \approx [\, (R - 1) + K_I^{1/2}\ (1 - \ln\varphi) / \kappa\,] / K_I^{1/2} \quad , \quad \varphi \le 1 \qquad (36)$$

which can be evaluated for a proscribed z_{HF} and $z_B = 1/ (2k_0)$ where k_0 is the peak wave number.

Similarly since normal to the wind stress (Section 3.2) the component of velocity is uniform, $v_{HF} = v_2$, and hence,

$$v_{HF}/w_* \approx - (R - 1)/ K_I^{1/2} \qquad (37)$$

from which, we obtain,

$$\gamma_{HF} = \tan^{-1}(v_{HF}/u_{HF}) \approx - \tan^{-1}\{ (R - 1)/ [(R - 1) + K_I^{1/2} (1 - \ln\varphi) / \kappa)]\}, \quad \varphi \leq 1 \qquad (38)$$

where γ_{HF} is the angle of deflection of the HF Radar mean drift to the surface shear stress. Note that (38) indicates that, if the HF Radar sampling is confined to the wave boundary layer, the maximum the angle of deflection ($\left|\gamma_{HF}\right|$) is 45^o.

The possible influence of the Ekman layer below can be investigated simply on the assumption that the Ekman depth (z_E) is much greater than the penetration depth of the HF Radar sampling into the Ekman layer, $z_3 = z_{HF} - z_B$, as would normally be expected. Then for $z_3/z_E << 1$, where $z_E = (f/2\upsilon_2)^{-1/2}$, $f > 0$, is the Ekman depth. On expressing ν_2 in terms of G and then eliminating G using (25) and (30), we obtain, $z_E = w_* K_I^{1/2} /(f(R-1))$. Hence the Ekman depth becomes infinite as $R \rightarrow 1$, and the components of mean velocity in the top region of the Ekman layer[1], $<u_3>$, $<v_3>$ are approximately, u_2 , v_2 , such that the speed factor of the HF Radar mean drift current along ox, with the inclusion of the contribution from the Ekman layer is

$$u_{HF} / w_* = [(R - 1) + \varphi^{-1} K_I^{1/2}/\kappa]/K_I^{1/2} \quad , \varphi > 1 \qquad (39)$$

from which using (37) we deduce that $\left|\gamma_{HF}\right| \rightarrow 45^o$, as the wave boundary becomes very shallow. The conclusion is that if the HF Radar measurements only extend into the top region of the Ekman layer, the cause of the existence of deflection angles greater than 45^o must be sought elsewhere.

---

[1] The exact expressions for the components of mean velocity in the Ekman layer are, $<u_3> = u_2 \exp(-z')\sin(z')/(z')$ and $<v_3> = v_2 [1 - \exp(-z') \cos(z')]/(z')$, where $z' = z_3/z_E$. For $z' \rightarrow 0$, $<u_3>$

$\rightarrow u_2$ and $\langle v_3 \rangle \rightarrow v_2$, and over the complete extent of the Ekman layer ($z' \rightarrow \infty$), the components of Ekman transport ($\underline{U}_E = \langle \underline{u}_3 \rangle z_3$) are $U_E = 0$, and from (37), $V_E = -(R-1)w_* z_E/K_I^{1/2}$, which, on eliminating z_E yields the classical expression, $V_E = -w_*^2/f$.

The velocity profiles in the Ekman layer are shown in Chereskin (1995) and also discussed in Jenkins and Bye (2006).

We recall now that the expressions for the HF Radar measurements obtained so far are due to the pure surface drift. The total HF Radar mean drift current is,

$$[\underline{u}_{HF}] = \underline{u}_{HF} + \underline{u}_o \qquad (40)$$

in which the angle of deflection,

$$[\gamma_{HF}] = \tan^{-1}\{[v_{HF} + v_o] / [u_{HF} + u_o]\} \qquad (41)$$

Eq. (41) can be used to examine the sensitivity of $[\gamma_{HF}]$ to u_o and v_o, which may be regarded as errors in the removal of the surface circulation from the data sets from which the drift parameters are obtained. We also emphasize that the theoretical results for the angle of deflection apply strictly to a steady-state neutral Ekman layer. Effects of density stratification in the coupled Ekman layers are not included.

5. Selected observational studies

The results of a variety of historical studies (Samuels and Huang 1982) have been inconclusive in achieving a consensus on the speed factor and angle of deflection for pure drift. Here we mention two studies, the results of which can be interpreted using the theoretical model presented in Section 4.

5.1 Drift card observations in the North Atlantic Ocean

An early drift card study in the North Atlantic Ocean (Hughes 1956) seems to have been the only example in which the surface drift was interpreted in terms of the surface geostrophic wind. Bundles of 10 drift cards enclosed in plastic envelopes were dropped from an aircraft every 10 nm and the shortest drift time following recovery was recorded, which ranged from 27 – 145 days over the 50 nm laying paths. The results showed that the drift of the envelopes, which occurred in an area where there was no evidence of 'well-defined permanent currents' was 'sensibly parallel to the isobars' with a drift speed of 2% of the wind speed.

These semi-quantitative observations are well predicted by the theoretical results that the pure surface drift lies along the direction of the surface geostrophic wind (21), and that the surface drift layer speed factor determined from (21), assuming that $u_d/u_s \approx 0.6$, see Section 4.1 (ii), is about $0.6 \times 0.034 \approx 2$ %. A thorough investigation of the near surface large scale drift circulation however awaits the development of satellite tracked surface drifters of thickness a few centimeters, which are surrogates for the depth mean current in the surface drift layer. The satellite tracked Surface Velocity Program drifters (Maximenko et al. 2009) which are drogued at 15m with a surface float and also are subject to a wind factor (Lumpkin and Pazos 2006), presently in use, may only be regarded as a 'blunt instrument' with respect to the velocity field of the surface drift layer.

5.2 HF Radar measurement of near surface currents

The best technique for the study of the velocity structure in the near surface layer at present appears to be HF Radar. The results of two important studies are discussed below.

A multi-year study was carried out during the period, August 2003 – February 2007 in the eastern channel of Tsushima Strait in which the surface geostrophic current was measured from

two sea level stations located across the channel and 10m analyzed winds were made available by the Japanese Meteorological Agency. The speed factors and deflection angles of the wind-driven flows at the sea surface were then obtained over a depth of about 1 – 2 m (z_{HF} = 2m) using HF [high frequency] Radar measurements (Yoshikawa and Masuda 2009). A running mean with a 3 day period was applied to the data from which the seasonal averages were obtained. It was also noted that running means from 3 – 10 days gave very similar results. No supporting wave data were presented, however this gap has been supplemented using monthly mean WaveWatch III data for T and u_{10} for 2010 at 34.5^{o}N, 130^{o}E. The HF Radar measurements showed a seasonal cycle in HF radar speed factor, which varied between 8 in winter during which from the WaveWatch III data T ≈ 6s, and 13 in summer during which T ≈ 4 s. In the speed factors, the water friction velocity was obtained from u_{10} using the drag formula of Yelland and Taylor (1996) which yielded a surface shear stress of 0.08 Nm^{-2} in winter and 0.06 Nm^{-2} in summer (Ide and Yoshikawa 2015), and in both seasons, $K_{10} = 1.1\ 10^{-3}$. The deflection angle to the right hand side of the surface shear stress ranged from about 22^o in winter to about 58^o in summer.

A second investigation occurred during the period, October 2006 –July 2008, in the Soya Strait (Zhang et al. 2015) in which the reference deep current was measured by a bottom mounted acoustic Doppler current profiler (ADCP) deployed about 18 km off the coast at about 45.6^{o}N, 142.1^{o}E in a water depth of 51 m, however the observations in this study do not have enough detail for a comparison with the results of the similarity model as is done below for the Tsushima Strait data.

In the Tsushima Strait, in winter, the depth of the wave boundary layer due to the wind sea, $z_B \approx$ 4.5 m so that the HF Radar mean drift lies well within the wave boundary layer since $z_{HF} < z_B$. In summer, however, if the wave boundary layer is controlled by the wind sea, the wave

boundary layer, is very shallow ($z_B \approx 2$ m) and the total HF Radar mean drift occurs throughout the wave boundary layer, and possibly also in the Ekman layer.

For the winter conditions, on substituting T = 6 s and $K_{10} = 0.0011$ in (12), we obtain R = 1.09, from which (32) yields $\gamma = -9^o$, and on substituting for R and φ in (36), we obtain $u_{HF}/w_* = 7$. The predicted speed factor is very similar to the observed value of 8, and, from (38), the predicted angle of the drift transport to the right hand side of the surface shear stress ($-\gamma_{HF}$) is 19^o , which is also close to the observed deflection angle of 22^o. We conclude that the similarity model is a satisfactory first order predictor of the winter HF Radar drift observations.

For the summer conditions, however, the situation appears more complex. On substituting T = 4 s ($z_B \approx 2$ m) and $K_{10} = 0.0011$, we obtain R = 1.01, $\gamma = -1^o$, $u_{HF}/w_* = 3$ and $\gamma_{HF} = -7^o$, which are very different from the observed values. Why is this? A possible explanation is that superimposed on the wind-sea, there is a dominant swell component, which sets the peak period (T) in (12). Let us speculate that T = 15s, then $z_B = 12$ m and hence R = 1.19, $u_{HF}/w_* = 12$, and $-\gamma_{HF} = 22^o$, which are much closer to the observed values although the theoretical angle of deflection of the pure surface drift can never be greater than 45^o. We note though that this theoretical restriction does not apply to the total HF Radar mean drift current (41). Relatively small perturbations of the transverse current can give rise to a significant scatter in its angle of deflection, which possibly may exceed 45^o. As an example, on adding a small transverse current of -12 mms^- to the winter observations, the components of the drift circulation ($\underline{u}_{HF}$), (48, -16 mms^{-1} ; $\gamma_{HF} = -19^o$) would become ([$\underline{u}_{HF}$], (48, -28 mms^{-1}) ; [γ_{HF}] = -30^o).

In summary, our analysis has shown that the wave field may have important effects on the properties of the drift circulation. These effects are quite distinct from the effects of thermal stratification which have been investigated in Ide and Yoshikawa (2015), who modelled the drift

observations using a large eddy simulation (LES) which incorporated the effects of the surface heat flux on the surface velocity without an explicit representation of the wave boundary layer. In reality both effects are probably important and need to be incorporated jointly in a future model of this important aspect of the ocean circulation. We emphasize that a comprehensive investigation requires excellent data sets of both the local forcing agents for the local drift circulation and also of the underlying geostrophic circulation of which the studies by the Japanese workers in the Tsushima Strait appear to be the best example.

6. Conclusions

The main purpose of this paper is to present the theory for modeling ocean surface drift in a global study on monthly and annual time scales, in the tradition of ocean general circulation modeling. This has been achieved using similarity models which encompass both the oceanic and atmospheric boundary layers. This is in contrast to the interpretation of environmental studies of the oceanic planetary boundary layer, e.g. Ardhuin et al.(2009), D'Asaro et al. (2014), using large eddy simulations (LES) which incorporate the Stokes drift and the effects of wave breaking in the downward transfer of momentum. However, in a LES case study in which u_{10} = 15 ms^{-1}, and c_o = 10.6 ms^{-1} (T = 6.8 s), the predictions for the surface drift current (longitudinal component 17 w_* and transverse component -3 w_*) which give rise to an angle of deflection of about 10^o (McWilliams et al. 2012) are similar to the predictions for the depth-mean surface drift current (iv) of the idealized case study in Section 4.1, which are derived from the similarity model. Thus it appears that the physics of the LES of the oceanic boundary layer is consistent with the existence of the similarity model.

The similarity model, which assumes a local dynamical equilibrium, and is supported on an underlying geostrophic circulation leads to expressions for the pure drift current in terms of both the 10m wind and the surface geostrophic wind under steady-state neutral conditions in both fluids. These conditions are likely to be approximately satisfied in the wave boundary layer over periods of averaging between 10 and 30 minutes over which the predictions for the 10m drag coefficient from the similarity theory are in excellent agreement with observational data (Bye et al. 2014). The results of the similarity model are a function of R which is specified by the friction velocity (u_*) and the peak wave period (T). In the Ekman layers, the period of averaging over which the similarity model is applicable is much longer, with the requirement that $R > 1$, which is necessary for a steady-state equilibrium in which the results of Section 3.4 apply. A global model for ocean drift on monthly and annual time scales therefore has an inbuilt mechanism for assessing the accuracy of the predictions obtained through the application of the similarity analysis to simultaneous fields of surface wind and surface geostrophic wind data. Note that over shorter periods of averaging the surface data may indicate that $R < 1$ in which event the Ekman response is necessarily transient.

The observational drivers for the computation of the component of pure drift (and the speed factor) from surface data are the fields of 10m wind velocity and the peak wave period, through which the frictional parameter (R) is determined. R also determines the angle of deflection of the pure drift to the 10m wind direction under equilibrium Ekman conditions. A notable result is that the angle of deflection is independent of the Earth's rotation since the Ekman vertical scales (u_*/f and w_*/f) occur in the similarity expressions for the fluid viscosities. In the air a logarithmic profile, which is local in height, is assumed in deriving the 10m drag law, and in the water, the

extension of the results for the sea surface drift to the depth mean drift is done on the assumption of the existence of a logarithmic current profile.

The most important product of this study is the development of a series of simple expressions for the properties of the drift field which are readily evaluated from wind and wave data fields. These expressions flow from the application of the inertial coupling relation (5) for the surface shear stress, which properly takes account of the presence of both the surface wind *and* the surface current in the dynamics of the air/sea coupled Ekman layers.

Glossary of Symbols

$\underline{u}(z)$ air velocity at height z

$\underline{u}(-z)$ water velocity at depth –z

oz vertically upward axis, undisturbed sea surface, z = 0

ρ_1 density of air

ρ_2 density of water, $\varepsilon = (\rho_1 \rho_2)^{1/2}$

$\underline{\tau}_s$ surface shear stress

$\underline{u}_* = (u_*, 0)$ friction velocity in air

$\underline{w}_* = (w_*, 0)$ friction velocity in water

$\underline{u}_L$ wave induced velocity in air (the spectrally weighted phase velocity)

$\varepsilon\underline{u}_L$ wave induced velocity in water (the surface Stokes velocity), which occur at $|z| = z_R$

$\underline{u}_o$ reference velocity for the air-sea boundary layer

$\underline{u}_1 = \underline{u}(z_B)$ surface wind

$\underline{u}_2 = \underline{u}(-z_B)$ surface current

$z_B = gT^2/8\pi^2$

T peak wave period

g acceleration of gravity

$\underline{u}_S$ surface drift velocity

u_{10} 10m wind speed, $z_{10} = 10$ m

κ von Karman's constant

$K = K(|z|)$ drag coefficient at $|z|$ in both fluids

$K_I = ¼\ K(z_B)$ inertial drag coefficient

R frictional parameter in the wave boundary layer, see Figure 1

$k_1 = 1/2z_R$ spectral high wave number cut-off

$k_o = 1/2z_B$ wave number of the peak wave

a_o amplitude of the breaking wave

Q_1 and Q_2 Ekman layer frictional coefficients in air and water respectively

υ_1 and υ_2 dynamic eddy viscosities in air and water respectively

$f > 0$ Coriolis parameter

G coefficient of non-dimensional eddy viscosity in the Ekman layers

$\underline{u}_g$ surface geostrophic wind

$\alpha = ½ /(R - 1)$ non-dimensional frictional parameter in the Ekman layers

K_o geostrophic drag coefficient

γ angle of turning of the surface geostrophic wind to the left hand side of the surface shear stress in the northern hemisphere

z_s roughness length for the velocity profiles at the sea surface

$\underline{u}_d$ mean drift current in the surface drift layer

z_{HF} depth sampled by the HF Radar measurements

z_3 penetration depth of the HF Radar measurements into the Ekman layer

z_E Ekman depth

$\varphi = z_{HF}/z_B$ the proportion of the wave boundary layer sampled by the HF Radar measurements

$\underline{u}_{HF} = (u_{HF}, v_{HF})$ HF Radar mean drift current

γ_{HF} angle of turning of the HF Radar mean drift current to the left hand side of the surface shear stress

$[\underline{u}_{HF}]$ total HF Radar mean drift current

$[\gamma_{HF}]$ angle of turning of the total HF Radar mean drift current to the left hand side of the surface shear stress

Acknowledgements JATB gratefully acknowledges the award of a Fellowship at the Hanse-Wissenschaftskolleg, Delmenhorst, Germany in the first half of 2013 during which this study was carried out in the Institute for Chemistry and Biology of the Sea (ICBM), University of Oldenburg. Informed comments by Professor Yutaka Yoshikawa and two other Reviewers are also especially acknowledged.

References

Andreas, E.L., Mahrt, L. and D. Vickers (2012) A new drag relation for aerodynamically rough flow over the ocean. J. Atmos. Sci. *69* 2520-2537 doi: 10.1175/JAS-D-11-0312.1

Ardhuin, F., Marie, L., Rascle, N., Forget, P. and A. Roland (2009) Observation and estimation of Lagrangian, Stokes and Eulerian currents induced by wind and waves at the sea surface. J. Phys. Oceanogr. *39* 2820-2838 doi: 10.1175/2009JPO 4169.1

Bye, J.A.T. (1965) Wind-driven circulation in unstratified lakes. Limnol. Oceanogr. *10* 451-458

Bye, J.A.T. (1987) Observations of drift velocity, wind and temperature profiles on the San Diego Model Yacht Pond (1965-1967). Cruise Rep. *12* Flinders Institute for Atmospheric and Marine Sciences, The Flinders University of South Australia

Bye, J.A.T. (1988) The coupling of wave drift and wind velocity profiles. J. Mar. Res. *46* 457-472

Bye, J.A.T. (1995) Inertial coupling of fluids with large density contrast. Phys. Lett. *A 202*, 222-224

Bye, J.A.T. (2002) Inertially coupled Ekman layers. Dyn. Atmos. and Oceans *35* 27-39

Bye, J.A.T. (2012) Southern Ocean surface drift: old observations and new theories Weather *67* 187-191

Bye, J.A.T. and J-O. Wolff (2004) Prediction of the drag-law for air-sea momentum exchange Ocean Dyn. *54* 577-580

Bye, J.A.T. and A.D. Jenkins (2006) Drag coefficient reduction at very high wind speeds. J. Geophys. Res. *111* C03024, doi:10.1029/2005JC003114

Bye, J.A.T. and J-O. Wolff (2008) Charnock dynamics: a model for the velocity structure in the wave boundary layer of the air-sea interface. Ocean Dyn. *58* 31-42

Bye, J.A.T and A.V. Babanin (2009) Wave generation by wind. Encyclopedia of Ocean Sciences (Second Edition). Steele, J.H., Turekian, K.K. and S.A. Thorpe (eds.) 304-309

Bye, J.A.T., M. Ghantous and J-O. Wolff (2010) On the variability of the Charnock constant and the functional dependence of the drag coefficient on wind speed. Ocean. Dyn. *60* 851-860

Bye, J.A.T., J-O. Wolff and K. A. Lettmann (2014) On the variability of the Charnock constant and the functional dependence of the drag coefficient on wind speed: Part II - Observations. Ocean Dyn. *64* 969–974 doi: 10.1007/s10236-014-0735-4

Chereskin, T.K. (1995) Direct evidence of an Ekman balance in the California Current. J. Geophys. Res. *100* 18261 - 18269

D'Asaro, E.A., Thomson, J., Shcherbina, A. Y., Harcourt, R.R., Cronin, M.F., Hemer, M.A. and B. Fox-Kemper (2014) Quantifying upper ocean turbulence driven by surface waves. Geophys. Res. Lett. *41* 1 - 6 doi: 10.1002/2013GL058193, 2014

Ekman, V.W. (1905) On the influence of the Earth's rotation on ocean-currents. Arkiv for Matematik, Astronomi och Fysik *2(11)* 1-52

Foreman,R.J. and S. Emeis (2010) Revisiting the definition of the drag coefficient in the marine atmospheric boundary layer. J. Phys. Oceanogr**.** *40* 2325-2332

Friehe, C.A., Smith, J.A., Rieder, K.F., Huang, N.E., Giovanangeli, J-P. and G.L. Geernaert (2001) Chapter 12 Wind, Stress and Wave Directions 232 – 241 *in* Wind Stress over the Ocean Ian S.F. Jones and Yoshiaki Toba (eds.) Cambridge University Press, Cambridge, 307 pp

Garratt, J.R. (1992) The Atmospheric Boundary Layer. Cambridge Univ. Press, Cambridge, 307 pp.

Geernaert, G.L. (1988) Measurements of the angle between the wind vector and wind stress vector in the surface layer over the North Sea. J. Geophys. Res. *93* 8215-8220

Hughes, P. (1956) A determination of the relation between wind and sea-surface drift. Quart. J.R. Met. Soc. *82* 494-502

Ide, Y. and Y. Yoshikawa (2015) Effects of diurnal cycle of surface heat flux on wind-driven flow. J. Oceanogr. online 04 November 2015, doi; 10.1007/s10872-015-0328-y

Jenkins, A.D. and J.A.T. Bye (2006) Some aspects of the work of V.W. Ekman Polar Record *42* 15-22 doi:10.1017/S00322347405004845

Lumpkin, R. and M. Pazos (2006) Measuring surface currents with Surface Velocity Program drifters: the instrument, its data, and some recent results. In Lagrangian Analysis and Prediction of Coastal and Ocean Dynamics (LAPCOD) A. Griffa, A.D. Kirwan, A.J. Mariano, T. Ozgokmen and T. Rossby (eds.)

Maximenko, N., Niiler, P., Centurioni, L., Rio, M.-H., Melnichenko, O., Centurioni, L., Chambers, D., Zlotnicki, V. and B. Galperin 2009 Mean dynamic topography of the ocean derived from satellite and drifting buoy data using three different techniques. J. Atmos. Ocean Tech. *26* 1910-1919

McWilliams, J.C., Huckle, E., Liang, J-H. and P. P. Sullivan (2012) The Wavy Ekman layer: Langmuir circulations, Breaking waves, and Reynolds stress. J. Phys. Oceanogr. *42* 1793 – 1816

Pond, S. and G.L. Pickard (1983) Introductory Dynamical Oceanography (2nd ed.) 329 pp

Rieder, K.F., Smith, J.A. and R.A. Weller (1994) Observed directional characteristics of the wind, wind stress and surface waves on the open ocean. J. Geophys. Res. *99* 22596 - 22598

Samuels, W.B. and N.E. Huang (1982) An oilspill trajectory analysis model with a variable wind deflection angle. Ocean Engng. *9* 347-360

Thorpe, S.A. (2004) Langmuir Circulation. Ann. Rev. Fluid Mech. *36* 55-79, doi:36.052203.071431

Yelland, M. and P.K. Taylor (1996) Wind stress measurements from the open ocean. J. Phys. Oceanogr. *26* 541-558

Yoshikawa, Y. and A. Masuda (2009) Seasonal variations in the speed factor and deflection angle of the wind-driven surface flow in the Tsushima Strait. J. Geophys. Res. *114* C12022, doi:10.1029/2009JC005632

Zhang. W., Ebuchi, N., Fukamachi, Y. and Y. Yoshikawa (2015) Estimation of wind drift current in the Soya Strait. J. Oceanogr. online 23 November 2015, doi: 10.1007/s10872-015-0333-1

List of Figures

1. The velocity structure in the wave boundary layer reproduced from Fig. 1 of Bye and Wolff (2008). The definitions of the variables are summarized in the Glossary.
2. (a) The frictional parameter (R) as a function of u_* and T, evaluated from equation (A1) in the Appendix of Bye et al. (2014) with $K_{10m} = 0.002$ and $u_{10m} = 40\ ms^{-1}$.

   (b) The speed factor (u_s/w_*) as a function of u_* and T, evaluated from (11) using the friction parameter (R) illustrated in Figure 2(a).
3. The angle of deflection (γ) as a function of u_* and T in the southern hemisphere, evaluated from (32) for $R \geq 1$, and assumed to be zero for $R < 1$.

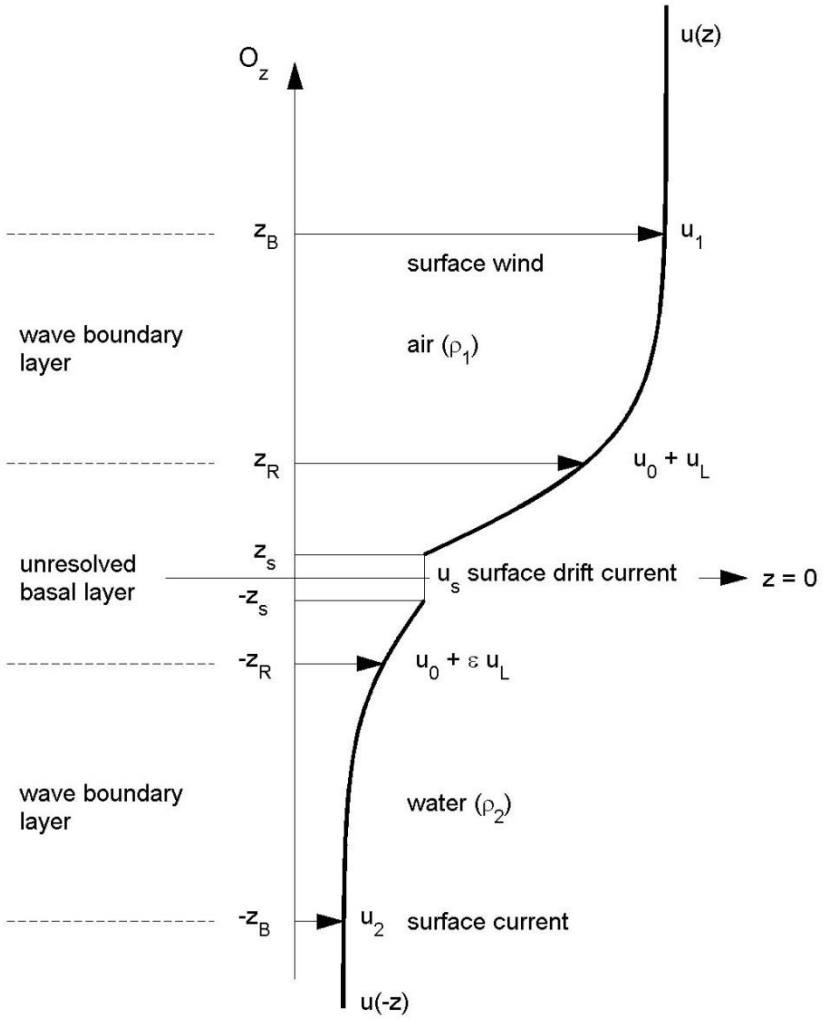

Fig. 1 The velocity structure in the wave boundary layer reproduced from Fig. 1 of Bye and Wolff (2008)

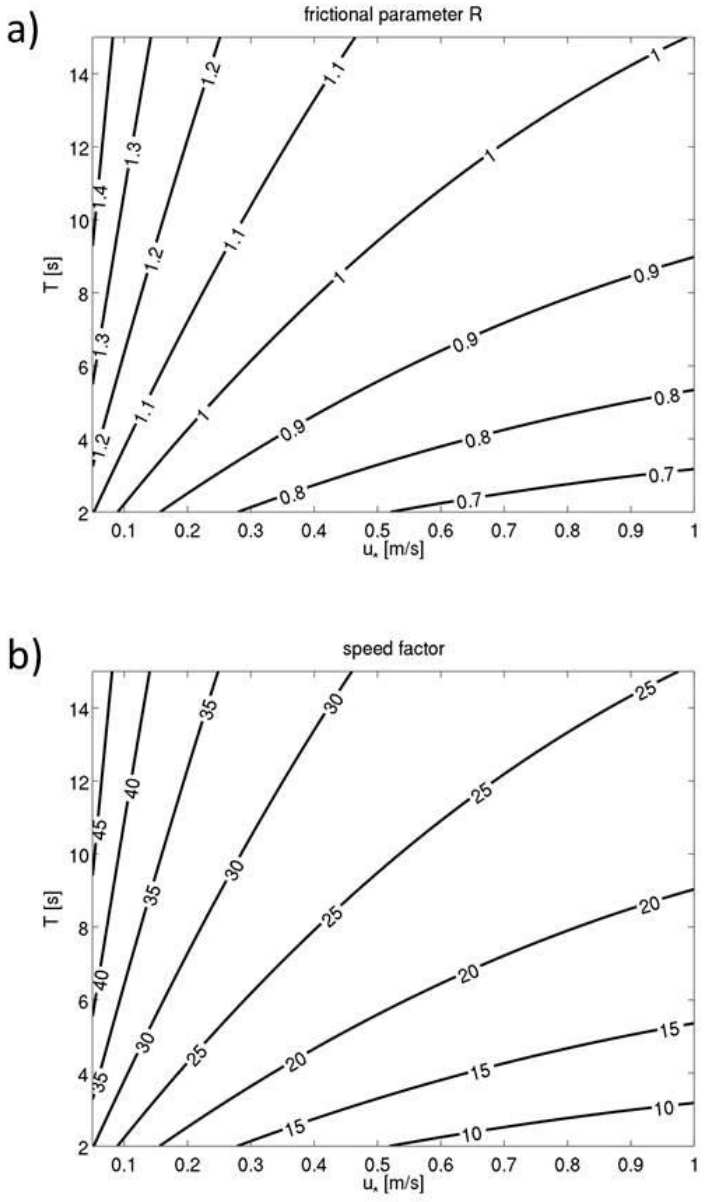

Fig. 2 (a) The frictional parameter (R) as a function of u_* and T, evaluated from equation (A1) in the Appendix of Bye et al. (2014) with $K_{10m} = 0.002$ and $u_{10m} = 40\ ms^{-1}$. (b) The speed factor (u_s/w_*) as a function of u_* and T, evaluated from (13) using the friction parameter (R) illustrated in Figure 2(a).

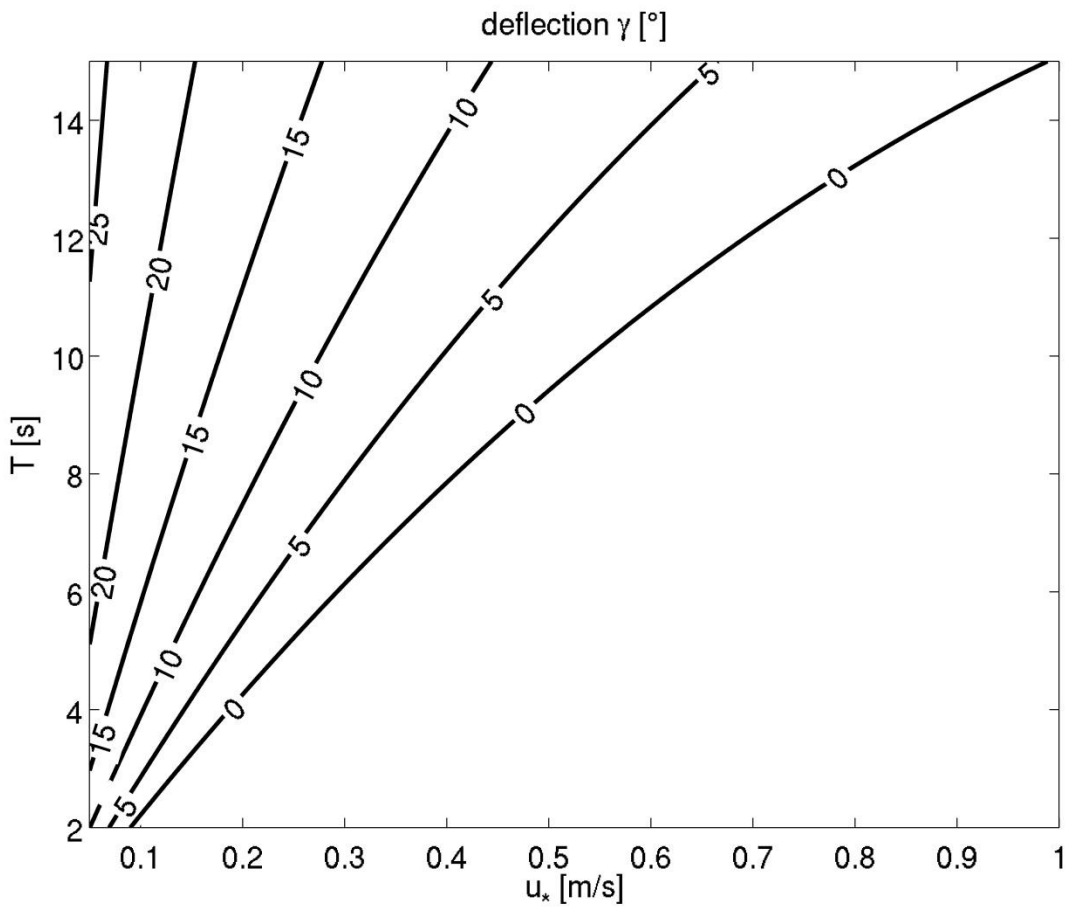

Fig. 3 The angle of deflection (γ) as a function of u* and T in the southern hemisphere, evaluated from (40) for $R \geq 1$, and assumed to be zero for $R < 1$.